Flow Behavior of Colloidal Rodlike Viruses in the Nematic Phase

M. Paul Lettinga*

IFF, Institut Weiche Materie, Forschungszentrum Jülich, D-52425 Jülich, Germany

Zvonimir Dogic

Rowland Institute at Harvard, Harvard University, Cambridge Massachusetts 02142

Hao Wang

Department of Physics, North Dakota State University, Fargo, North Dakota 58105

Jan Vermant

Department of Chemical Engineering, Katholieke Universiteit Leuven, de Croylaan 46, B-3001 Leuven, Belgium

The behavior of a colloidal suspension of rodlike *fd* viruses in the nematic phase, subjected to steady state and transient shear flows, is studied. The monodisperse nature of these rods combined with relatively small textural contribution to the overall stress make this a suitable model system to investigate the effects of flow on the nonequilibrium phase diagram. Transient rheological experiments are used to determine the critical shear rates at which director tumbling, wagging, and flow-aligning occurs. The present model system enables us to study the effect of rod concentration on these transitions. The results are in quantitatively agreement with the Doi−Edwards−Hess model. Moreover, we observe that there is a strong connection between the dynamic transitions and structure formation, which is not incorporated in theory.

I. Introduction

When subjected to shear flow, liquid crystals can exhibit a variety of surprising phenomena, which arise because of the anisotropic shape of the constituent rods. Theoretically, the behavior of a suspension of hard rods during shear flow can be described by the equation that governs the time development of their probability distribution function, as derived by Hess[1] and by Doi and Edwards.[2] In the absence of a flow, the Doi−Edwards−Hess (DEH) theory reduces to the Onsager description of equilibrium nematic liquid crystals and can be used to describe the isotropic−nematic (I−N) phase transition of a hard rod suspension.[3] The rheological properties are predicted to be highly nonlinear functions of the Péclet number (*Pe*), which is the ratio of shear rate $\dot{\gamma}$ over rotational diffusion constant D_r. This is not surprising as the *Pe* number can be much larger than unity when the rodlike molecules have large aspect ratios.

The nonlinear response of the rheological properties indicates that the shear flow distorts the equilibrium distribution of macromolecules or rods. The spatiotemporal microstructural changes during flow are even more complex. At low shear rates, the DEH theory predicts that the pseudo vector describing the average alignment of the rods, i.e., the "director", undergoes a continuous "tumbling" motion in the plane defined by the velocity and the velocity gradient vectors. At high shear rates the director is predicted to align with the flow.[4,5] At intermediate shear rates, it is possible to obtain multiple solutions to the Doi−Edwards-Hess equation, which are dependent on the initial orientation of the director.[6,7] For one stable solution called "wagging" the nematic director oscillates between two angles in the plane defined by the flow and the gradient of the flow. Other solutions such as kayaking and log-rolling are also possible, in which the director oscillates out of the flow-gradient plane at these intermediate shear rates.[8]

Experiments on polymeric liquid crystals have confirmed several predictions of the Doi−Edwards equation. Using a combination of rheological and rheo-optical measurements, it was shown that nematic solutions of poly(benzyl-glutamate) (PBG) tumble at low shear rate and become flow aligning at high shear rates.[9] The existence of a wagging regime and a potential coexistence of wagging and log-rolling regimes at intermediate flow rates have also been revealed in experiments.[8,10] However, there remain significant difficulties when comparing experiments on polymeric liquid crystals (PLC) to theoretical predictions. One problem is that different levels of

---

* To whom correspondence should be addressed.

(1) Hess, S. Fokker-planck-equation approach to flow alignment in liquid crystals. *Z. Naturforsch.* **1976**, *31* (a), 1034−1037.

(2) Doi, M.; Edwards, S. F. *The Theory of Polymer Dynamics*; Clarendon Press: Oxford, U.K., 1986.

(3) Onsager, L. The effect of shape on the interaction of colloidal particles. *Ann. N.Y. Acad. Sci.* **1949**, *51*, 62−659.

(4) Marrucci, G.; Maffettone, P. L. Description of the liquid-crystallin phase at high shear rates. *Macromolecules* **1989**, *22*, 4076.

(5) Larson, R. G. Arrested tumbling in shearing flows of liquid crystal polymers. *Macromolecules* **1990**, *23*, 3983−3992.

(6) Faraoni, V. Grosso, M.; Crescitelli, S.; Maffettone, P. L. The rigid-rod model for nematic polymers: An anaysis of the shear flow problem. *J. Rheol.* **1999**, *43*, 829.

(7) Forest, M. G.; Wang, Q. Monodomain response of finit-aspect-ratio macromolecules in shear and realted linear flows. *Rheol. Acta* **2003**, *42*, 20−46.

(8) Grosso, M.; Crescitelli, S.; Somma, E.; Vermant, J.; Moldeaers, P.; Maffettone, P. L. Prediction and observation of sustained in a shear liquid crystalline polymer. *Phys. Rev. Lett.* **2003**, *90*, 098304.

(9) Burghardt, W. R.; Fuller, G. G. Role of director tumbling in the rheology of polymer liquid crystal solutions. *Macromolecules* **1991**, *24*, 2546.

(10) Mewis, J.; Mortier, M.; Vermant, J.; Moldenaers, P. Experimental evidence for the existence of a wagging regime in polymeric liquid crystals. *Macromolecules* **1997**, *30* (5), 1323−1328.

the microstructure may lead to different contributions to the stress tensor.[11] In addition to the molecular contribution to the stress tensor, textural aspects contribute. The latter include Frank elasticity contributions due to the presence of spatial distortions of nematic director and viscous interactions between "domains". In addition, there is an indirect effect to the stress tensor as the defects disturb the orientation distribution function. These textural contributions to the total stress dominate the behavior at high concentrations and low shear rates,[12] making it difficult to accurately extract information about the concentration dependence of different flow transitions. The textural portion of the stress typically displays scaling of the transient rheological response with strain rather than with *Pe* number.[13] The strain scaling is a typical feature of materials where the time response is determined by an inherent length scale which in the case of PLCs is set by the size of the large non-Brownian nematic domains.[14]

The DEH theory describes the flow behavior of a homogeneous ensemble of rods but does not consider any polydomain effects. Therefore, an ideal system for testing DEH theory should have small textural contributions. In this paper, we use rodlike *fd* virus suspensions to access the concentration dependence of the transition of tumbling to wagging and wagging to flow aligning. We show that the contribution of textural stress is very low, although the spatial distribution of directors still has to be accounted for. The main motive for using *fd* virus is the thorough understanding of its equilibrium behavior, which has been quantitatively described using the Onsager theory extended to take into account the semiflexible nature of *fd* as well as its surface charge.[15] Moreover, *fd* has already successfully been used for (micro)rheology experiments in the isotropic phase.[16,17] The aim of the present paper is to make a comparison between the *dynamic* flow behavior of *fd* suspensions and the available *microscopic* theoretical predictions of the DEH theory for a homogeneous system of colloidal rods under shear.

The paper is organized as follows. In section II, we discuss the equation of motion of the orientational distribution function and the numerical method we use to solve it. The experimental details about sample preparation and measurements are given in section III. The results are discussed in five parts: the stationary viscosity of *fd* suspensions, the concentration and shear rate dependence of the oscillatory response to a flow reversal, the relaxation after cessation of flow at high concentration, and in situ microscopy under shear. In section IV, the textural contribution to the stress tensor is investigated in more detail. Finally, we present a nonequilibrium phase diagram of shear and concentration dependence of different flow transitions.

II. Theory

The distribution of an ensemble of rods can be described by the probability density function $P(\hat{\mathbf{u}}_1,.., \hat{\mathbf{u}}_N, \mathbf{r}_1,.., \mathbf{r}_n)$ of the positions $\{\bar{\mathbf{r}}_i\}$ and orientations $\{\hat{\mathbf{u}}_i\}$ of the rods. Ignoring any spatial correlations, i.e., restricting to a monodomain, we have $P(\hat{\mathbf{u}}_1,.., \hat{\mathbf{u}}_N, \mathbf{r}_1,.., \mathbf{r}_n) = \bar{\rho} P(\hat{\mathbf{u}}_1,.., \hat{\mathbf{u}}_N)$, where $\bar{\rho} = N/V$ is the particle density. Therefore, the *orientational* probability density function, or orientational distribution function (ODF), fully characterizes the system. The time evolution of the ODF for a suspension of rods during flow is obtained by solving the equation of motion for the ODF, given by the *N*-particle Smoluchowski equation

$$\frac{\partial P(\hat{\mathbf{u}}, t)}{\partial t} = D_r \mathscr{R} \cdot \{ \mathscr{R} P(\hat{\mathbf{u}}, t) + DL^2 \bar{\rho} P(\hat{\mathbf{u}}, t) \hat{\mathscr{R}} \oint d\hat{\mathbf{u}}' P$$
$$(\hat{\mathbf{u}}', t) |\hat{\mathbf{u}}' \times \hat{\mathbf{u}}| \} - \hat{\mathscr{R}} P(\hat{\mathbf{u}}, t) \hat{\mathbf{u}} \times (\Gamma \cdot \hat{\mathbf{u}}) \quad (1)$$

where $\mathscr{R}(...) = \hat{\mathbf{u}} \times \nabla_{\hat{\mathbf{u}}}(...)$ is the rotation operator with respect to the orientation $\hat{\mathbf{u}}$ of a rod. D_r is the rotational diffusion of a rod at infinite dilution. Furthermore, D is the thickness of the rods and L is their length. $\Gamma = \dot{\gamma} \hat{\Gamma}$ is the velocity-gradient tensor with $\dot{\gamma}$ the shear rate. Here we choose

$$\hat{\Gamma} = \begin{pmatrix} 0 & 1 & 0 \\ 0 & 0 & 0 \\ 0 & 0 & 0 \end{pmatrix} \quad (2)$$

which corresponds to a flow **v** in the *x*-direction and its gradient $\nabla \mathbf{v}$ in the *y* direction.

The concentration where the isotropic phase becomes unstable *in the absence of shear flow* can be calculated by solving the Smoluchowski equation at zero shear rate. This equation agrees with Onsagers approach to the I−N transition. Often the Maier-Saupe potential is used instead of the exact potential, which in fact corresponds to the first term of the Ginzburg-Landau expansion of the outer product in the exact potential given between the brackets in eq 1.[18] Under *flow conditions*, a rich dynamics phase behavior is found as a function of shear rate and rod concentration. Marrucci and Maffettone were the first to solve the equation of motion of the ODF numerically, restricting themselves to two dimensions in order to reduce the computational effort.[4] They found that the director undergoes a tumbling motion with respect to the flow direction, resulting in a negative normal stress N_1. Larson expanded the ODF in three dimensions using spherical harmonics and truncated the expansion after checking for convergence.[5] This treatment predicts a transition from tumbling to "wagging" and finally to flow aligning state with increasing shear rates. A closure relation is frequently used for the interaction term on the right side of eq 1. This can greatly bias the results, see e.g., Feng et al.[19] The location of the flow transitions in the flow-concentration diagram is very sensitive to the choice of the closure, and no satisfactory closure has been found up till now.

In this paper, we use a finite element method to numerically solve the equation of motion for the ODF, thus avoiding the use of any specific closure relation. As a typical diffusion−convection equation, eq 1 describes the diffusive−convective transport dynamics of an ori-

(11) Larson, R. G. On the relative magnitudes of viscous, elastic and texture stresses in liquid crystalline PBG solutions. *Rheol. Acta* **1996**, *35* (2), 150−159.

(12) Walker, L. M.; Mortier, M.; Moldenaers, P. Concentration effects on the rheology and texture of pbg/*m*-cresol solutions. *J. Rheol.* **1996**, *40* (5), 967−981.

(13) Moldenaers, P.; Mewis, J. Transient behavior of liquid crystalline solutions of poly(benzylglutamate). *J. Rheol.* **1986**, *30* (1), 567−584.

(14) Larson, R. G.; Doi, M. Mesoscopic domain theory for textured liquid crystalline polymers. *J. Rheol.* **1991**, *35* (4), 539−563.

(15) Purdy, K. R. Dogic, Z.; Fraden, S.; Rühm, A.; Lurio, L.; Mochrie, S. G. J. Measuring the nematic order of suspensions of colloidal fd virus by X-ray diffraction and optical birefringence. *Phys. Rev. E.* **2003**, *67*, 031708.

(16) Graf, C. Kramer, H.; Deggelmann, M.; Hagenbüchle, M.; Johner, Ch.; Martin, Ch.; Weber, R. Rheological properties of suspensions of interacting rodlike fd-virus particles. *J. Chem. Phys.* **1993**, *98* (6), 4921−4928.

(17) Schmidt, F. G.; Hinner, B.; Sackmann, E.; Tang, J. X. Viscoelastic properties of semiflexible filamentous bacteriophage *fd*. *Phys. Rev. E* **2000**, *62* (4), 5509−5517.

(18) Dhont, J. K. G.; Briels, W. J. Viscoelasticity of suspensions of long, rigid rods. *Colloid Surf. A* **2003**, *213* (2−3), 131−156.

(19) Feng, J.; Chaubal, C. V.; Leal, L. G. Closure approximations for the doi theory: Which to use in simulating complex flows of liquid-crystalline polymers? *J. Rheol.* **1998**, *42* (5), 1095−1119.
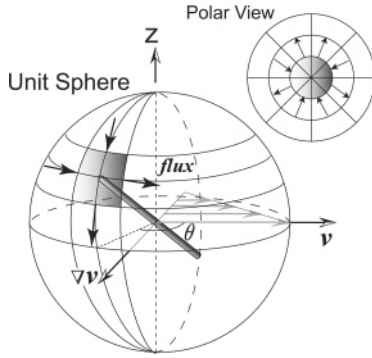
Figure 1. Flux conservation method used in discritizing eq 1. The rod indicates the orientation of the director with respect to the shear flow. The probability of finding a tip of one rod in the shaded area of the unit sphere is determined by the flux of the probabilities through the boundary of that area.

entation of a homogeneous ensemble of thin rigid rods. A surface of a sphere is constructed on which a tip of the rod moves with respect to its center of mass. The equation for the probability of finding the tip of a rod in an area is determined by the transport fluxes on its boundaries due to (1) the Brownian diffusion (the first term in the brace brackets of eq 1), (2) the convection induced by the interparticle forces (the second term in the brace brackets of eq 1), and (3) the convection due to the imposed shear flow (the third term of eq 1).

To solve eq 1 numerically, a discretization scheme is used, and meshes on the surface of a unit sphere are constructed. For those operators inside the brace brackets which represent the transport fluxes, we apply the central differences approximations. However, the rotation operator outside of the brace brackets needs to be discretized using the concept of transport fluxes through the boundaries of the mesh. In other words, the integral form of the eq 1 is invoked and applied to each of the mesh elements. To do this the identity, $(\hat{\mathbf{u}} \times \nabla_{\hat{\mathbf{u}}}) \cdot \mathbf{F} = \nabla_{\hat{\mathbf{u}}} \cdot (\mathbf{F} \times \hat{\mathbf{u}})$ is used in order to transform the angular transport flux of a rod to the translational transport flux of one tip of that rod. It differs from the conventional method of discretizing a differential equation where the operators are written explicitly into the sum of the first- and second-order derivatives, and then the latter are approximated by selected difference schemes. The advantage of the current method is that, since neighboring meshes share boundaries, the fluxes leaving one mesh are always absorbed by the surrounding meshes and vice versa. Therefore, there is no loss and generation in the total amount of the ODFs as the computation proceeds (see Figure 1). In practice, a 40×80 mesh was used on the surface of a unit sphere with 40 equispaced grids in the polar angle and 80 equispaced grids in the azimuthal angle in a spherical coordinates. The right-hand side of eq 1 is discretized on the meshes according to the flux-conservative method mentioned above. A fourth order Adams' predictor-corrector method[20] was invoked to follow the time evolution of the ODF. More details will be published in a forthcoming paper.

The time-dependent ODF is now used to calculate the time-dependence of three parameters characterizing the flow behavior of a nematic phase: (1) θ describing the angle between the nematic director and flow direction, (2) the scalar magnitude of the director defined by the order

parameter P_2, and (3) the total stress of an ensemble of flowing rods. The angle and magnitude of the order parameter are obtained from the order parameter tensor

$$\mathbf{S} = \oint d\hat{\mathbf{u}} \ \hat{\mathbf{u}}\hat{\mathbf{u}}P(\hat{\mathbf{u}}, t) \tag{3}$$

The largest eigenvalue of the order parameter tensor λ, characterizes the degree of alignment of rods with respect to the director given by the corresponding eigenvector $\hat{\boldsymbol{n}}$. The largest eigenvalue of $\mathbf{S}$ is $1/3$ in the isotropic phase and 1 for a perfectly aligned nematic phase. Scalar order parameter P_2 is defined as $P_2 = (3\lambda - 1)/2$.

The stress σ_{12} is obtained from the deviatoric part of the stress tensor derived by Dhont and Briels[18]

$$\Sigma_D = \eta_0 \dot{\gamma} +$$
$$3\bar{\rho}k_B T \left\{ \mathbf{S} - \frac{1}{3}\hat{\mathbf{I}} + \frac{L}{D}\phi\Sigma_I^D + \frac{1}{6}Pe_r\left[\mathbf{S}^{(4)}: \ \hat{\mathbf{E}} - \frac{1}{3}\hat{\mathbf{I}}\mathbf{S}: \ \hat{\mathbf{E}}\right]\right\} \tag{4}$$

where

$$\Sigma_I^D = \frac{8}{3\pi}\oint d\hat{\mathbf{u}}\oint d\hat{\mathbf{u}}'\hat{\mathbf{u}}\hat{\mathbf{u}} \times \frac{\hat{\mathbf{u}} \times \hat{\mathbf{u}}'}{|\hat{\mathbf{u}} \times \hat{\mathbf{u}}'|}\hat{\mathbf{u}}\cdot\hat{\mathbf{u}}'P(\hat{\mathbf{u}}, t)P(\hat{\mathbf{u}}', t) \tag{5}$$

and

$$\mathbf{S}^{(4)} = \oint d\hat{\mathbf{u}} \ \hat{\mathbf{u}}\hat{\mathbf{u}}\hat{\mathbf{u}}\hat{\mathbf{u}}P(\hat{\mathbf{u}}, t) \tag{6}$$

Here, $\phi = \pi/4 \ D^2L\bar{\rho}$ is the volume fraction of rods, and $Pe = \dot{\gamma}/D_r$ the rotational Péclet number which is defined as the shear rate scaled with the rotational diffusion of a rod at infinite dilution. The first term between the brackets, $\mathbf{S} - 1/3\hat{\mathbf{I}}$, stems from the Brownian contribution to the stress. The second term stems from the direct interaction between rods and describes the elastic contribution to the total stress. The proportionality constant $\phi L/D$ is the dimensionless rod concentration and is also called the nematic strength. The terms proportional to $\sim Pe_r$ stem from the flow of the suspension and described the viscous contribution to the total stress. This term disappears instantaneously when the shear is switched off.

In Figure 2, we plot the evolution of the three parameters (angle θ, order parameter P_2, and stress σ_{12}) as a function of strain for different shear rates at a dimensionless rod concentration of $\phi L/D = 4.5$. For this calculation, we used an initial rod orientation in the flow-gradient plane. The flow behavior between Péclet numbers of 4.5 and 5.0 exhibits a sharp transition from tumbling behavior, where the director continuously rotates, to wagging behavior where the director hops back and forth between two well defined angles. At higher shear rates, the director is found to be flow aligning. The order parameter at low shear rates remains unchanged, but is significantly reduced at the point of the tumbling to wagging flow transition.

III. Materials and Methods

The viscosity and stress response were measured using an ARES strain controlled rheometer (TA instruments, Delaware). A double wall Couette geometry was used because of the fairly low viscosity of the samples. Polarized light microscopy images of *fd* under shear flow were taken using a Linkam CSS450 plate-plate shear cell.

The physical characteristics of the bacteriophage *fd* are its length $L = 880$ nm, diameter $D = 6.6$ nm, persistence length of 2200 nm, and a charge per unit length of around 10 e$^-$/nm at pH 8.2.[21] When in solution, *fd* exhibits isotropic, cholesteric, and

(20) Korn, G. A.; Korn, T. M. *Mathematical Handbook for Scientists and Engineers*; Mc-Graw and Hill: New York, 1968.

(21) Fraden, S. *Observation, Prediction, and Simulation of Phase Transitions in Complex Fluids*, volume 460 of *NATO-ASI − Series C*; Baus, M.; Rull, L. F.; Ryckaert, J. P., Eds.; Kluwer Academic Publishers: Dordrecht, The Netherlands, 1995; pp 113−164.
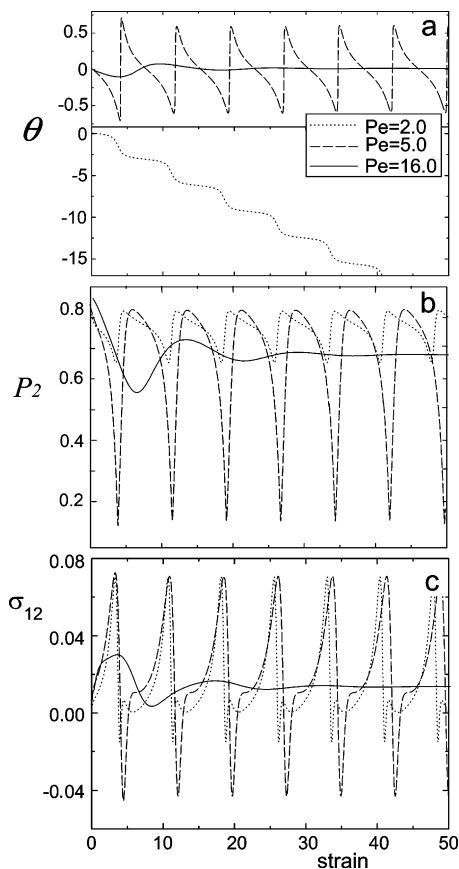
Figure 2. Three plots showing the behavior of the angle of the nematic director θ (a), the magnitude of the nematic order parameter(b), and the average stress (c) as a function of strain after a start up of the flow. The dimensionless rod concentration is $\phi\,L/D$ = 4.5. Data are obtained by numerically solving eq 1 using the finite element method. The rods are initially placed in the flow-gradient plane. For the stress calculation only the elastic contribution (eq 4) was considered.

smectic phases with increasing concentration.[22,23] *fd* forms a cholesteric phase while the DEH theory is valid for nematic structures. In practice, nematic and cholesteric phase are locally almost identical and the free energy difference between these phases is very small.[24] In this paper, we do not distinguish between these two phases. The *fd* virus was prepared according to standard biological protocols using XL1-Blue strain of *E. coli* as the host bacteria.[25] The standard yields are approximately 50 mg of *fd* per liter of infected bacteria, and virus is typically grown in 6 L batches. The virus is purified by repetitive centrifugation (108 000 g for 5 h) and re-dispersed in a 20 mM Tris-HCl buffer at pH 8.2.

A. *fd* as a Model Hard Rod System. The Onsager theory for hard rod dispersions predicts a first order phase transition between a disordered, isotropic phase and an orientationally ordered, nematic phase. Due to hard core athermal interactions considered in the Onsager model, the phase diagram is temperature independent and the rod concentration is the only parameter that determines the location of the I−N phase transition. The two points spanning the region of isotropic−nematic coexistence are called the binodal points. The spinodal point is located at a rod concentration higher than the lower
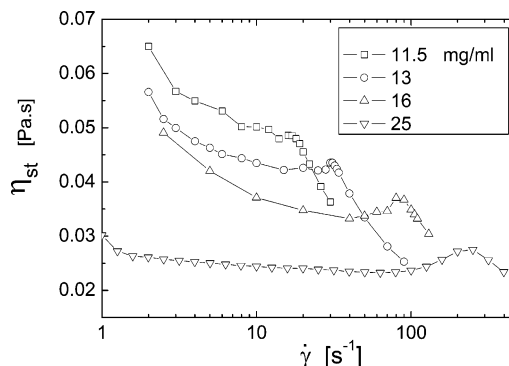

Figure 3. Stationary viscosity as a function of shear rate for four different concentration of *fd* virus at 11.5, 13, 16, and 25 mg/mL.

binodal point and is determined by the following condition $\phi\,L/D$ = 4. *fd* viruses are not true hard rods, due to surface charge and limited flexibility. As a consequence, their equilibrium phase behavior differs from the ideal hard rod case described by Onsager based theory, e.g., DEH. The finite flexibility of *fd* viruses drives the concentration of the binodal points to a 30% higher value when compared to equivalent but perfectly stiff hard rods. In addition, flexibility also reduces the value of the order parameter of the coexisting nematic phase. For *fd*, the order parameter of the coexisting nematic is about 0.65, whereas Onsager theory for hard rods in equilibrium predicts the order parameter of 0.8.[15] The effect of surface charge is to increase the effective diameter of the rod D_{eff} and therefore the excluded volume interaction between charged rods. As a consequence, the charge reduces the real concentration of the phase transition.[26]

For the *fd* suspension used, the binodal point at high rod concentration c_{IN} occurs at 11 mg/mL. After taking the effects of flexibility and charge into account, it was shown that the order parameter of the nematic solution of *fd* is quantitatively described by the extensions of the Onsager theory to the semiflexible case.[15] Hence, even though *fd* is flexible and charged, it can be used to quantitatively test predictions of the DEH theory. It is, however, a very difficult and until now unfulfilled task to incorporate charge and flexibility into a nonequilibrium equation of motion such as eq 1. Therefore, in this paper, we use data from ref 15 to convert the measured concentration of *fd* to the nematic order parameter of the sample. After that, we compare experiments and theory at the same values of the order parameter.

IV. Results

A. Stationary Viscosity. The measurements of a stationary viscosity as a function of the shear rate for different *fd* concentrations are shown in Figure 3. For the lowest concentrations of *fd*, the viscosity decreases continuously with shear rate except for a small hesitation at a shear rate of 10 s^{-1}. This hesitation is similar to what is observed for solutions of PBG at low concentration in solvent *m*-cresol.[13,27] For *fd* at intermediate concentrations, shear thinning becomes less pronounced, the hesitation shifts to higher shear rates and turns into a local maximum. For the highest *fd* concentration, almost no shear thinning is observed, only a pronounced peak in the viscosity. This shear thickening behavior has not been previously reported.

A hesitation in the shear rate dependence of the viscosity was predicted theoretically by Larson.[5] It was argued that the transition from the tumbling regime to the wagging regime implies a broadening of the ODF which leads to higher dissipative stresses. The broadening of the ODF

(22) Dogic, Z.; Fraden, S. Smectic phase in a colloidal suspension of semiflexible virus particles. *Phys. Rev. Lett.* **1997**, *78*, 2417.

(23) Dogic, Z.; Fraden, S. Development of model colloidal liquid crystals and the kinetics of the isotropic-smectic transition. *Philos. Trans. R. Soc. London A* **2001**, *359*, 997.

(24) Dogic, Z.; Fraden, S. Cholesteric phase in virus suspensions. *Langmuir* **2000**, *16*, 7820−7824.

(25) Sambrook, J.; Fritsch, E. F.; Maniatis, T. *Molecular Cloning: A Laboratory Manual*, 2nd ed.; Cold Spring Harbor Laboratory Press: Plainview, NY, 1989; Chapter 4.

(26) Tang, J.; Fraden, S. Isotropic-cholesteric phase transition in colloidal dispersions of filamentous bacteriophage *fd*. *Liq. Cryst.* **1995**, *19* (4), 459−467.

(27) Kiss, G.; Porter, R. S. Rheolgy of concentrated solutions of poly-(γ-benzyl-glutamate). *J. Polym. Sci.* **1978**, *65*, 193−211.
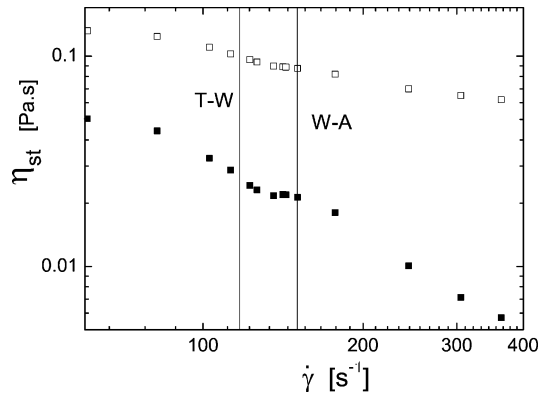
Figure 4. Theoretical time averaged viscosity at a dimensionless concentration of $L/D\ \phi = 4.5$ with ($\square$) and without ($\blacksquare$) the viscous contribution of the rods, as calculated by solving the equation of motion of the ODF for 20 independent initial orientations of the director. The lines indicate the transition from tumbling to wagging, and from wagging to flow aligning as found from Figure 2. The results are scaled to the experiment using a typical concentration of 16 mg/mL for $\bar{\rho}$ in eq 4 and $D_{\text{inf}}^0 = 20\ s^{-1}$ for the rotational diffusion at infinite dilution.[15,28]

is illustrated in Figure 2b. As can be seen in Figure 2c, it is not straightforward that ODF broadening really has an effect on the stress. We calculated the time-dependent viscosity by numerically solving the equation of motion of the ODF for 20 different initial orientations of the director. From the time-dependent ODFs, we calculated the viscosity using either only the elastic term or both elastic and viscous terms. The viscosity is averaged over all 20 traces and a tumbling period after the transient start up flows have died out. The results are scaled to the experiment using a typical concentration of 16 mg/mL for $\bar{\rho}$ in eq 4 and the value of $D_{\text{inf}}^0 = 20\ s^{-1}$, taken for the rotational diffusion at infinite dilution.[15,28] In Figure 4 the stationary viscosity decreases continuously with increasing shear rate and only shows a hesitation when the viscous contribution to the stress is not included. The shear rate where this hesitation occurs corresponds with the shear rate where the system nematic ordering is significantly reduced and the transition from tumbling to wagging takes place, as can be concluded from Figure 2. Comparing the model predictions to the experiments, it should be noted that the experimentally observed features are much more pronounced. Moreover, there is no real reason to leave out the viscous contribution although it does obscure the behavior we see in the experiment. Still, the maximum in the viscosity is interpreted as a signature of the transition from tumbling to a wagging state.

There are three observations to keep in mind when considering *fd* in the nematic phase under shear flow, which all point to very low stresses in such systems when compared to polymeric liquid crystals. First, the viscosity of *fd* in the nematic phase is two to 3 orders of magnitude lower than the viscosity of typical polymeric liquid crystals such as poly(benzyl glutamate) (PBG),[29] although the difference in solvent viscosity is only 1 order of magnitude. Second, the range over which the viscosity of *fd* suspension varies is more limited with changing shear rate and rod concentration: the viscosity lies between 70 times the sol-
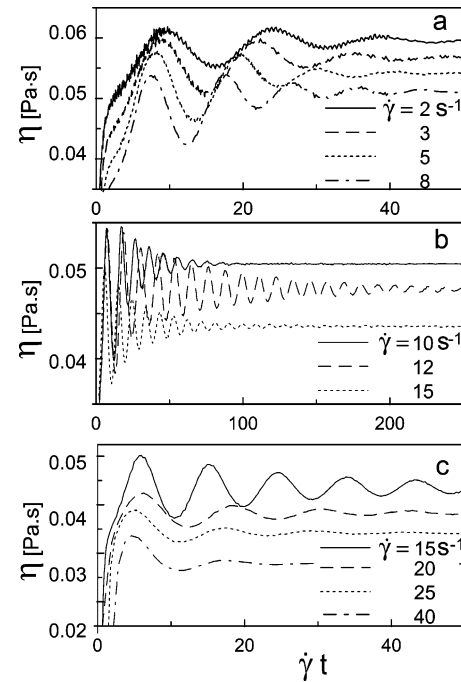
(28) Kramer, H. Deggelmann, M.; Graf, C.; Hagenbtichle, M.; Johner, C.; Weber, R. Electric birefringence measurements in aqueous fd virus solutions. *Macromolecules* **1992**, *25*, 4325−4328.

(29) Vermant, J.; Moldenaers, P.; Picken, S. J.; Mewis. J. A comparison between texture and rheological behaviour of lyotropic liquid crystalline polymers during flow. *J. Non-Newtonian Fluid Mech.* **1994**, *53*, 1−23.
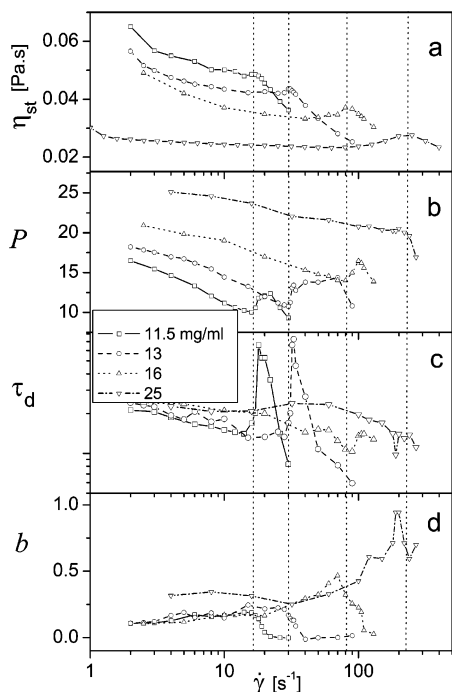

Figure 5. Viscosity of the nematic *fd* solution in a response to a flow reversals. The sample is sheared at shear rate $+\dot{\gamma}$ until the viscosity is equilibrated; at time $t = 0$ the shear rate is changed to $-\dot{\gamma}$. The concentration of *fd* is kept constant at 11.5 mg/mL. The data can be nicely fitted to eq 7. The fits are not shown for clarity.

vent viscosity for low shear rate and low rod concentration and 20 times the solvent viscosity for high shear rate and rod concentration. Moreover, the viscosity as calculated from the equation of motion of the ODF is of the same order as the measured viscosity. Third, polymer nematics exhibit negative first normal stress differences for certain shear rates as was first observed for PBG solution.[26] This is a direct consequence of the tumbling of the nematic director. Attempts have been made to measure the first normal stress difference for nematic *fd* solutions but due to very low force the signals were too small to be measured.

B. Flow Reversal Experiments. In flow reversal experiments, the sample is first sheared at a constant shear rate in one direction until the steady state condition is reached. Subsequently, the direction of flow is suddenly reversed while keeping the magnitude of shear rate constant. Such experiments have been very useful in characterizing and understanding the dynamics of sheared liquid crystalline polymers.[13] In the present work, flow reversal experiments were performed covering a wide range of shear rates and *fd* concentrations. Typical flow reversal experiments are depicted in Figure 5 for a *fd* concentration of 11.5 mg/mL which corresponds to $c/c_{\text{IN}} = 1.05$. At the lowest shear rates, a damped oscillatory response is obtained which decays within few oscillations (Figure 5a). Increasing the shear rate results in a more pronounced oscillatory response, which damps out relatively slowly. The oscillatory response in Figure 5b is most pronounced at a shear rate of $12\ s^{-1}$. At even higher shear rates, the damping again increases (Figure 5c). To quantitatively characterize the response of a nematic to a flow reversal, the data is fitted to a damped sinusoidal superimposed onto a asymptotically decaying function of the following form:

$$\eta(t) = \eta_{\text{stat}}\left\{1 + Ae^{-\dot{\gamma}t/\tau_d}\sin\left(2\pi\frac{\dot{\gamma}t - \varphi}{P}\right)\right\}(1 - bg^{\dot{\gamma}t}) \quad (7)$$

Figure 6. (a) Steady-state viscosity as function of the shear rate for *fd* virus at four different concentrations. All viscosity curves exhibit shear thinning at low shear rates followed by a local maximum in viscosity. (b−d) Behavior of the parameters obtained from fitting the response of the shear flow reversal experiments to eq 7. The vertical lines indicate the local maximum in viscosity curves. The local maximum in the steady-state viscosity curve corresponds to maximum of the tumbling period P and damping constant τ_d and minimum of asymptotic constat b in the flow reversal.

This is an empirical choice, but each variable in the fit contains important information about the behavior of rods in shear flow. Figure 6 shows the behavior of fit parameters as a function of the shear rate at few selected concentrations of *fd* virus. In this figure, we indicate with vertical dashed lines the shear rates at which the steady state viscosity exhibits a local maximum for four different concentrations. Interestingly, these are exactly the same shear rates at which the damping constant τ_d as well as the tumbling period P show a sharp increase. The asymptotic constant b, on the contrary, shows a decrease. These features disappear for the highest *fd* concentration. Presumably the three regions showing different flow reversal behavior correspond to tumbling, wagging and flow aligning regime. This will be discussed in more detail in section V.B. In the next section. we first discuss the concentration and shear rate dependence of the tumbling period in the regime where rods exhibit tumbling flow behavior.

C. Tumbling Period as a Function of Shear Rate and Rod Concentration. DEH theory predicts that as the *De* (or *Pe*) number is increased, that the "molecular" period of oscillation decreases with increasing shear rate in the tumbling regime.[5] This feature was never fully explored, since in most polymeric liquid crystals it was found that the tumbling period was strain scaling, implying that the response overlaps when the period is scaled with the applied shear rate and the stress is normalized by its steady state value. The strain scaling arises as a consequence of the presence of a large, non-Brownian, length scale in the sample that determines the time response, even at relatively high *De* (or *Pe*) numbers. This most probably is the domain size characterizing the nematic texture. The log−log plot of the tumbling period ($T = P/\dot{\gamma}$) as a function of the shear rate is shown in Figure
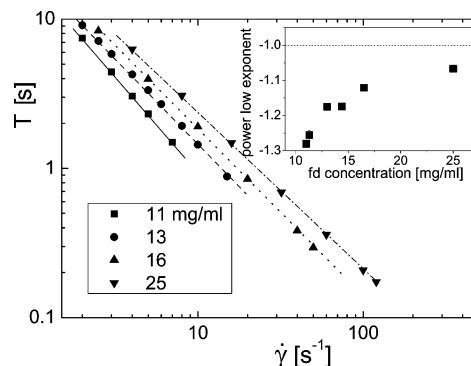

Figure 7. Dependence of the tumbling periods on the shear rate for different concentrations of the nematic *fd*. The figure shows that the tumbling period scales with a power low as a function of the shear rate. The inset shows the power law dependence of the tumbling period on the shear rate for different *fd* concentrations.
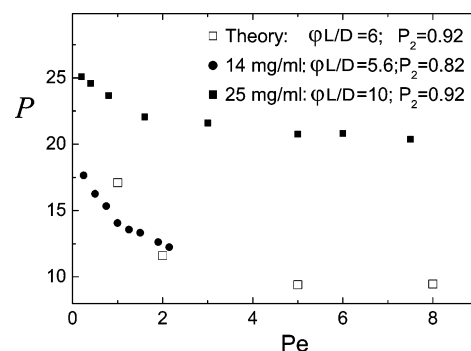

Figure 8. Period of the oscillations (in units of strain) as a function of the Péclet number, where the shear rate is scaled with the rotational diffusion of *fd* at infinite dilution.

7. Here the data are only shown for a low shear rate region which is associated with the tumbling region. Strain scaling, if present, would give a slope of −1. However, as can be seen in the inset of Figure 7, the reciprocal indicating strain scaling is only approached and not reached at the highest rod concentration studied here.

The shear rate dependence of the tumbling period is compared to the theoretical prediction for the same rod concentration as well as the same order parameter, see Figure 8. The reason for using the order parameter to assess the theoretical predictions was discussed at length in section III.A. For purposes of comparison, the order parameter was obtained from X-ray experiments and the value of $D_{inf}^0 = 20$ s^{-1}. We emphasize that DEH theory is microscopic and that there are no adjustable parameters in the comparison between theory and experiments. Clearly there is a qualitative correspondence between theory and experiment, both showing a continuous decrease of the period. The quantitative correspondence, on the other hand, is limited. This is probably due to fact that texture, although not dominating the response, is still present. It will be shown later in section V.B that the shear rate and rod concentration dependence of a tumbling to wagging and wagging to flow-aligning transition agree much better with DEH theory.

The concentration dependence of the tumbling period is shown in Figure 9. Here, theory and experiments are compared at a fixed shear rate at which the tumbling to wagging flow transition occurs. The tumbling period increases with increasing rod concentration (Figure 9a) or, equivalently, increasing order parameter of the nematic phase (Figure 9b). The increase of the tumbling period
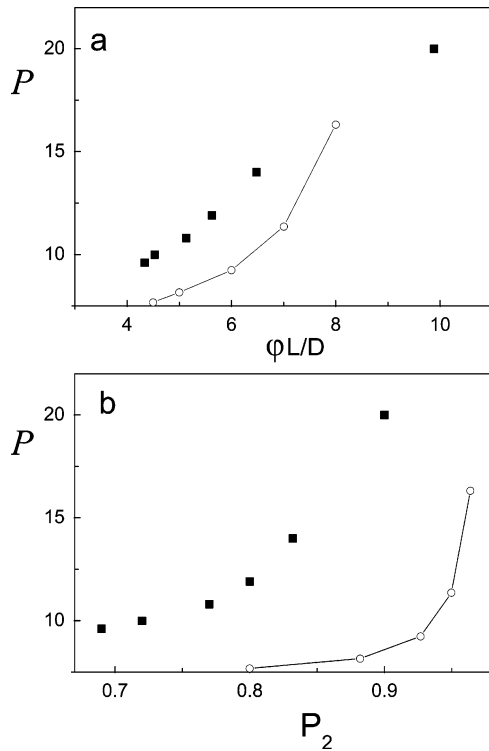
Figure 9. Period of the oscillations (in units of strain) as a function of the dimensionless concentration (a) and order parameter (b). The shear rate was chosen at the point we identify with the tumbling to wagging transition for experiment (■) and exact theory (○).
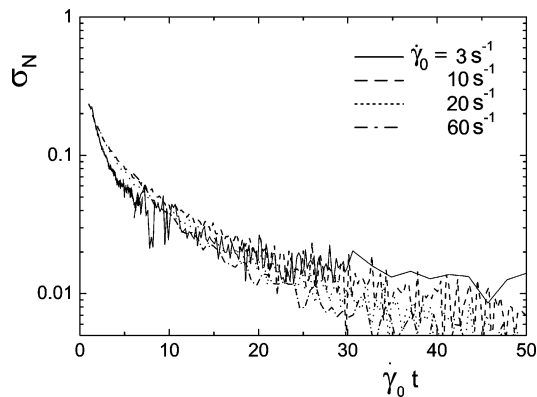

Figure 10. Stress relaxation after cessation of flow for *fd* at 25 mg/mL ($c/c^* = 2.3$), varying the initial shear rate. The time is scaled by the initial shear rate. The stress is normalized by the stress before the cessation of flow.

with increasing order parameter was already predicted using a linearized version of the DEH theory.[30]

In conclusion, the absence of strain scaling of the tumbling period and the qualitative agreement between theory and experiment the tumbling period indicates that the response of the suspension of *fd* virus is dominated by the molecular elasticity arising from the distortion of the ODF of particles.

D. Relaxation at High Concentration. To measure the relative magnitude of the elastic texture contribution to the overall stress, relaxation experiments were performed. For polymeric liquid crystals such as polybenzylglutamate (PBG) solutions in *m*-cresol, Walker et al.[12] showed that there are three different regimes of relaxation behavior, each of which is related to a distinct structural

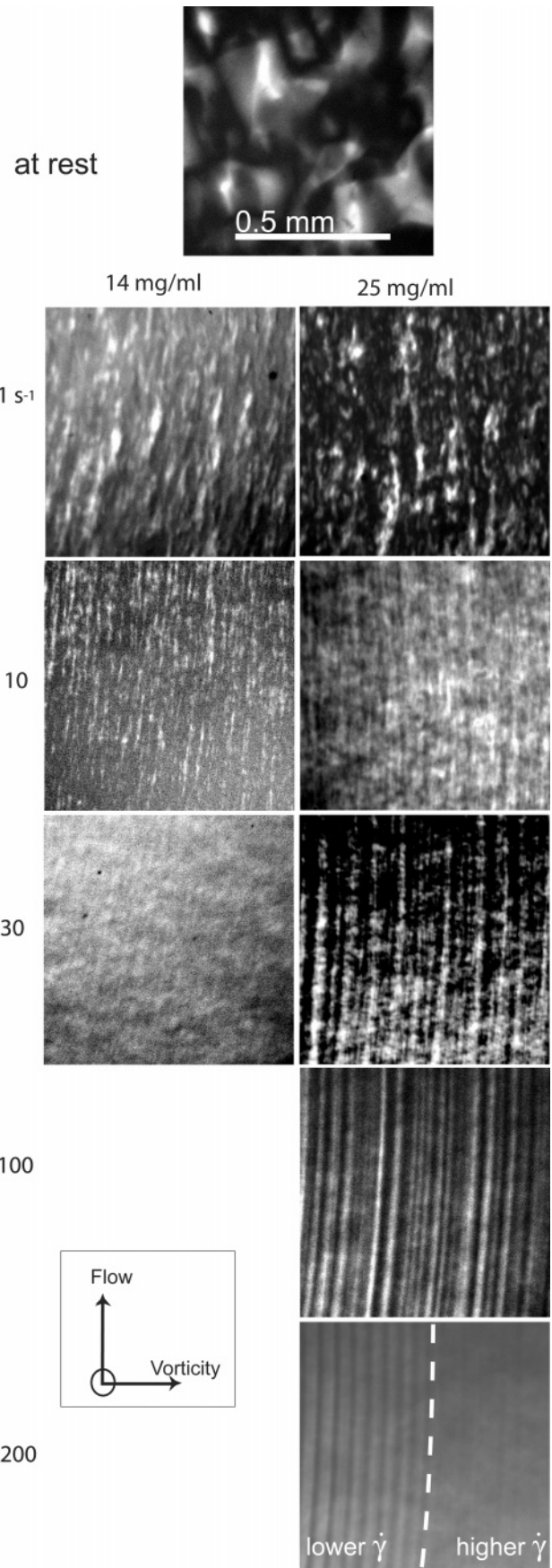(30) Kuzuu, N.; Doi, M. *J. Phys. Soc. Jpn.* **1984**, *53*, 1031.

Figure 11. Polarization images of the nematic *fd* at 14 and 25 mg/mL for a range of different steady-state shear rates. The dashed line in the bottom right image indicates the border between the structured and unstructured regions.

relaxation. There is a "fast" relaxation of the nematic fluid; a "slower" relaxation that exhibits scaling with the shear rate before the cessation of flow, which is due to the indirect contribution of the texture to the overall stress; and a "long-time" relaxation due to the reorganization of the texture on a supramolecular level which will not be addressed here.

Stress relaxation experiments were performed in the low shear rate "tumbling" region, at shear rates smaller than those corresponding to the maximum in the viscosity. The sample used had a relatively high *fd* concentration of 25 mg/mL, corresponding with $c/c_{IN} = 2.3$. Some typical responses to the cessation of flow are depicted in Figure 10. The stress is normalized to its value before the cessation of flow, and the time axis is scaled by the shear rate. The fast component of the decay takes place at less than a tenth of a second, which is comparable to the response of the force re-balanced transducer and therefore not shown. The slow component of the stress relaxation scales when time is multiplied with the previous shear rate, but only from the point that the stress has decayed to less than 30% of its original value, or less for higher initial shear rates. From Figure 10, it can be concluded that the contribution to the stress for the highest concentration used and for low shear rates is 30%. This is the absolute upper limit for the samples used in this paper. It should be noted that for PBG solutions 30% it was found to be the lower limit.[12]

E. In Situ Microscopy. The flow-induced changes of the liquid crystalline texture during steady-state shear flow were studied using a plate–plate geometry in combination with a polarization microscope. Measurements were performed for *fd* concentrations of 14 and 25 mg/mL. Typical images are shown in Figure 11 for different shear rates. Interestingly the characteristic size of the "domains" was very large. Birefringent regions of up to half a millimeter were observed under static conditions. When the sample is subjected to shear flow, these domains will elongate and eventually disappear, at values of the shear rate which correspond to the maximum in the viscosity (see Figure 6a). An important difference between the two concentrations is that the elongated domains merge into bands for high rod concentration, whereas for the low concentration the structure disappears before such bands are formed. Interestingly, this transition to a banded structure in the high concentration fluid takes place at a shear rate which is higher than the shear rate where the low concentration fluid loses its features.

V. Discussion

When comparing the flow behavior of the polymeric nematic phase and the colloidal nematic phase of the dispersed *fd* viruses, the most striking observation is the qualitative agreement between the two systems, despite the fact that *fd* is 1 order of magnitude larger. The viscosity of the *fd* nematic is much smaller, and the rotational diffusion of *fd* is much slower when compared to polymeric liquid crystals. Flow reversal experiments reveal typical transitions in the transient rheological behavior: damped oscillations occur at low shear rates changing to undamped oscillations at intermediate shear rate, which disappear if the shear rate is increased even further; the time scale of the oscillations of the stress transients is comparable. Also other well-known phenomena like the formation of very large bands upon cessation of flow along the vorticity direction which have been studied in detail in polymeric systems[31] can also be observed here (data not shown).

Having established that *fd* virus dispersions indeed undergo a tumbling motion under flow, the *dynamic* behavior of *fd* suspensions can be rationalized on the basis of the microscopic theoretical predictions for a homogeneous system of rods under shear. Doing so, one important prerequisite needs to be fulfilled, namely that the dominating contribution to the stress is coming from the nematic fluid and not from the texture. It will be argued here that this indeed is the case. Having done so, we will be able to map out a phase diagram of the dynamic transitions from tumbling to wagging to flow aligning.

A. Textural Evolution during Flow. The word "texture" refers to disclination points and lines where the director of the nematic phase changes discontinuously, marking domains in the sample. When a system containing these domains and disclinations is subjected to shear flow, part of the dissipated energy is used to destroy these structures. Figure 11 shows that the domains tend to elongate and align with the flow. Disclinations can also cause a direct contribution to the total stress resulting in a high viscosity and a very pronounced shear thinning behavior, typically referred to as region I.[32] Experiments on polymeric liquid crystals have revealed several features of the flow behavior of nematic liquid crystals which are attributed to the presence of texture in the nematic phase. Tumbling induces distortions in the director field and the defects arrest the tumbling, thereby inducing an elastic stress. The length scale over which this distortion occurs, i.e., the "domain" length scale, is an inherent non-Brownian length scale, see ref 33. As a consequence, stress patterns during flow reversal will display strain scaling. Also the damping of the oscillations is explained on the base of the presence of the polydomain structure, where, e.g., the "friction" between the domains would lead to a damping of the oscillations.[14,34] The scaling of the stress relaxation process after the flow is stopped with shear rate has been explained using the same arguments. From such an experiment, the relative contribution to the total stress of a homogeneous nematic phase and the polydomain texture can be estimated since the relaxation dynamics of the nematic phase is much faster than that of polydomain structure.[12]

The micrographs in Figure 11 clearly reveal that texture under flow exists in nematic *fd* dispersions. Their contribution to the rheology is, however, far less prominent when compared to polymeric liquid crystals such as PBG. This we can infer from several observations. First, very moderate shear thinning is observed in the low shear rate regime for the *low* concentrations, which gradually disappears with increasing concentration (Figure 6b). This is very similar to theoretical predictions for a homogeneous nematic phase (Figure 2b in ref 18). Also, the calculated and measured viscosities are of the same order of magnitude. In contrast, shear thinning can be fairly strong in the low shear rate region (region I) where texture dominates the response, and it will increase with increasing concentration,[35] although also other microstructural

(31) Vermant, J.; Moldenaers, P.; Mewis, J.; Picken, S. J. Band formation upon cessation of flow in liquid-crystalline polymers. *J. Rheol.* **1994**, *38* (5), 1571–1589.

(32) Walker, L. M.; Wagner, N. J. Rheology of region i flow in a lyotropic liquid-crystal polymer: The effects of defect texture) under shear and during relaxation. *J. Rheol.* **1994**, *38* (5), 1524–1547.

(33) Burghardt, W. R.; Fuller, G. G. Transient shear flow of nematic liquid crystals: Manifestations of director tumbling. *J. Rheol.* **1990**, *34* (6), 959–992.

(34) Kawaguchi, M. N.; Denn, M. M. A mesoscopic theory of liquid crystalline polymers. *J. Rheol.* **1999**, *43* (1), 111–124.

(35) Marrucci, G.; Greco, F. Flow behavior of liquid crystaline polymers. *Adv. Chem. Phys.* **1993**, *86*, 331.

features can contribute here.[36] Second, the tumbling period is not strain scaling (Figure 7), which could be due to either a smaller relative magnitude of the textural stress or due to the fact that we are not in a low enough *Pe* regime. Third, "strain" scaling is recovered for the slow "textural" relaxation process after the flow has been stopped. This experiment shows that at the highest rod concentrations used and at low shear rates the distortional textural contribution is about 30%. For most experiments done, this value is probably significantly lower. So, where texture is important, even dominating the stress response for molecular LCPs, molecular elasticity is far more dominating the *fd* virus. Though we just argued that the texture does not dominate the shear response of the system, this does not mean that the shear response is not influenced by texture. For one, the oscillations we observe are still strongly damped, and the damping only decreases when the transition to the flow aligning state is reached (see the behavior of τ_d in Figure 6). Moreover, the presence of texture might explain the discrepancy in the behavior of the period of the oscillations between experiment and theory (Figure 9). Most importantly, we know from microscopy that texture is present under shear (see Figure 11). It should be noted, however, that the size of the polydomain structure of the *fd* dispersions is 1 order of magnitude bigger as compared to PBG,[29] so that the density of disclination lines and points is about 3 orders of magnitude lower for *fd*. Note that the length scale of the texture during flow is still small compared to the dimension of the flow cell. Since the contribution of texture scales with the density of the disclinations,[35] texture will be far more dominating for e.g. PBG than for *fd*, even when elastic constants are almost the same for the two systems.[24,37]

B. Phase Diagram of Dynamical Flow Transitions. In this section, the experimental results are combined and a nonequilibrium phase diagram of *fd* rods under shear flow is presented. The results for the four fit parameters plotted in Figure 6 show clear transitions at well-defined shear rates for all *fd* concentrations. Although they only give an indirect proof of the transitions, they can be used to infer information about the flow transitions. For all *fd* concentrations (except for the highest one) the shear rate where the maximum viscosity is reached is identical with the shear rate where the period as well as the damping constant start to increase (indicated by the vertical dashed lines in Figure 6). The microscopic observations are in fairly good agreement with the transitions inferred from the rheology. Upon approaching the tumbling to wagging transition from tumbling to flow aligning, the texture becomes too faint to resolve in the microscope and texture subsequently disappears upon reaching the FA region. For the high *fd* concentration, i.e., the sample showing shear banding (Figure 11 last), one can identify a sharp transition from a structured to an unstructured region in the same micrograph. Since this picture was taken in the plate−plate geometry, there is a shear rate distribution across the image: the shear rate is increasing going from the left side to the right. A sharp spatial transition therefore also represents a sharp transition at a given shear rate. Although, due to the method of zero gap-setting, the value of the shear rate is not exactly known (±20%), one can still identify the shear

(36) Ugaz, V. M.; Cinader, D. K.; Burghardt, W. R. Origins of region I shear thinning in model lyotropic liquid crystalline polymers. *Macromolecules* **1997**, *30* (5), 1527−1530.
(37) Taratuta, V. G.; Hurd, A. J.; Meyer, R. B. Light-scattering study of a polymer nematic liquid crystal. *Phys. Rev. Lett.* **1985**, *55* (2), 246−249.
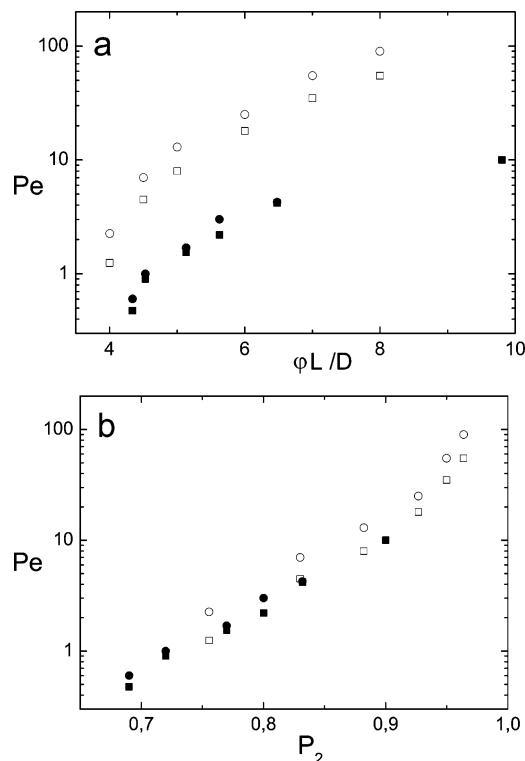

Figure 12. Phase diagram of flow transitions for the nematic *fd* phase as a function of dimensionless concentration (a) and order parameter (b). The experimental points indicate the Péclet numbers where the viscosity shows a local maximum (9) and where the damping constant τ_d (●) reaches a maximum. The theoretical points indicate tumbling to wagging (□) and wagging to flow aligning (○) transitions.

rate where structure disappears as the shear rate where the viscosity reaches its local maximum (the down pointing triangles in Figure 6a). For low *fd* concentration of (14 mg/mL) the structure disappears around the point where the viscosity reaches its local maximum, although the morphological transition for the lower concentration is less abrupt.

Figure 12 shows the behavior of flow transitions as a function of shear rate for various *fd* concentrations. For the experiment, we plotted the Péclet numbers where the viscosity shows a local maximum and where the damping constant reaches a maximum. The theoretical predictions for the tumbling to wagging and wagging to flow aligning transitions are obtained from the plots of the angle of the nematic director θ under flow, see Figure 2. Similar to the method used in Figure 9, the experimental concentration is scaled to the theoretical concentration in two different ways: effective concentration (Figure 12a) and the order parameter P_2 (Figure 12b). This figure was shown in a preliminary paper without a detailed explanation.[38] The shear rate is rescaled to the Péclet number by using the rotational diffusion coefficient at infinite dilution. Figure 12 allows us to draw some important conclusions. First, it is clear that scaling the concentration with the equilibrium order parameter gives better agreement when compared to the scaling by the dimensionless concentration. The fact that theory and experiment agree without using any fitting parameters (P_2 was obtained in a separate experiments[15]) leads to the conclusion that the DEH theory describes the flow behavior of the *fd* nematics quite well,

(38) Lettinga, M. P.; Dhont, J. K. G. Nonequilibrium phase behavior of rodlike viruses under shear flow. *J. Phys.: Condens. Matter* **2004**, *16*, 3929.

as long as the effects of flexibility and charge of the experimental rods are included in the calculation of the order parameter. A less convincing agreement is obtained when comparing the experimental and theoretically calculated periods (Figure 9). The reason for this could be the remaining textural contribution to the overall stress which, although small, cannot be neglected. Since we deduce from Figure 12b, that a dimensionless concentration of $\phi L/D = 4$ corresponds with a *fd* concentration of 16 mg/mL, we used this number a posteriori to scale the calculated molecular viscosity in Figure 4. The pure elastic contribution shows a very nice quantitative correspondence with the experimental data. Interestingly, when the viscous term is added, the theoretical viscosity is higher than the experimental viscosity, despite of the fact that no hydrodynamics is incorporated.

In the previous subsection, it was argued that the influence of textural contribution to the stress tensor of *fd* are relatively small, as compared to PLCs. There are however strong indications that the dynamic behavior is influenced by the macroscopic bands which are formed for the samples at the highest concentrations used (see Figure 11 end). As can be seen in Figure 6, the typical features for the transition to wagging disappear: there is no increase in the damping constant, nor in the period of the oscillations. Moreover, the theory shows only a moderate hesitation of the stationary viscosity (which even disappears when the viscous term is added, Figure 4), whereas in experiments a local peak is observed which is more pronounced with increasing concentration. The microscopy pictures show that at high concentrations the systems finds another way to handle the distortion of the particle distribution at high shear rates by forming shear bands where the overall orientational distribution is alternating, as was already observed and partially explained for the polymeric systems.[29,39,40] In the present work, the concentration dependence of the phenomenon at hand suggests that this merits further experimental as well as theoretical work. In this context, one should not forget that we compare experiments on charged and semiflexible *fd* with theory for hard and stiff rods. It could well be that these factors also play an important role. It will be a major challenge especially to take the semiflexibility into account in the equation of motion.

VI. Conclusions

Colloidal suspensions of rodlike *fd* viruses are an ideal model system to study the behavior of the nematic liquid crystalline phase under shear flow. Flow reversal experiments show signatures for tumbling, wagging, and flow

aligning behavior, very similar to the behavior found in polymeric liquid crystals. The rigid rod nature of the *fd* suspension, possibly combined with a smaller relative textural contributions to the overall stress tensor make *fd* virus a suitable model system for the DEH theory. Important in this respect is that the overall viscosity is only one to 2 orders of magnitude higher than the solvent viscosity. Also it is important to note that stress relaxation experiments combined with the absence of strain scaling in flow reversal experiments suggest that there is only a limited contribution of textural aspects to the overall stress, even for the highest *fd* concentration used in this work. The shear thickening of the viscosity observed for a range of *fd* concentrations is as yet, unexplained. The maximum in the viscosity occurs at the critical shear rate where the tumbling to wagging transition takes place. Microscopic observations show that at this shear rate the morphological features disappear, suggesting a strong connection between the dynamic transitions and structure formation.

The experimental results have been compared to a microscopic theory for rod like molecules subjected to shear flow. A nonequilibrium phase diagram is constructed, describing the transitions from tumbling to wagging and from wagging to flow-aligning as a function of rod concentration and applied shear stress. When scaling the results to the concentration where the isotropic−nematic transition takes place, the experiment and theory show only a qualitative agreement, possibly due to the fact that the real rods are are both semiflexible and charged. However, when scaling the results using the order parameter, which is determined by the interactions between the rods, theory and experiment show an excellent agreement without using any fit parameters. Thus, it can be concluded that the DEH theory accurately captures the dynamic features of a hard rod system. *fd* dispersions constitute such a hard rod system as long as flexibility and charge are properly taken into account, which can be simply achieved by using the order parameter to scale the data. More theoretical work is needed, however, to explain the clear connection between the observed band formation at high concentrations and the dynamic transitions, and to incorporate the effect of flexibility of the rods.

(39) Larson, R. G. Roll-cell instabilities in shearing flows of nematic polymers. *Liq. Cryst. 37* (2), 175−197.
(40) Larson, R. G.; Mead, D. W. The ericksen number and deborah number cascades in sheared polymeric nematics. *Liq. Cryst.* **1993**, *5*(2), 151−169.